

1 Historical and future trends in South Asian monsoon 2 low pressure systems in a high-resolution model 3 ensemble

4 **S. Vishnu** ^{†1,*}, **William R. Boos**^{1,2}, and **William D. Collins**²

5 ¹Department of Earth and Planetary Science, University of California, Berkeley, CA, USA

6 ²Climate and Ecosystem Sciences Division, Lawrence Berkeley National Laboratory, Berkeley, CA, USA

7 *vishnuedv@gmail.com

8 ABSTRACT

Historical trends in monsoon low pressure systems (LPS), the dominant rain-bearing weather system of South Asia, have been difficult to assess due to changes in the observing network. Future projections have also remained uncertain because prior studies concluded that many coarse-resolution climate models do not accurately simulate LPS. Here, we examine changes in South Asian monsoon LPS simulated by an ensemble of global models, including some with high spatial resolution, that we show skillfully represent LPS. In the ensemble mean, the number of strong LPS (monsoon depressions) decreased over the last 65 years (1950–2014) by about 15% while no trend was detected for weaker LPS (monsoon lows). The reduction in depression counts then moderated, yielding no trend in the periods 1980–2050 or 2015–2050. The ensemble mean projects a shift in genesis from ocean to land and an increase in LPS precipitation of at least 7%/K, which together contribute to a projected increase in seasonal mean and extreme precipitation over central India.

10 **Keywords:** HighResMIP, Low Pressure System, Extreme events, Trend, South Asia

11 1 Introduction

12 South Asia is home to the world's largest human population densities and most extreme rainfall, with societal infrastructure that
13 is highly vulnerable to hydrological extremes^{1,2}. Yet most projections of precipitation changes over the next century rely on a
14 set of global climate models that produce questionable simulations of the region's dominant rain-bearing weather system: the
15 monsoon low pressure system (LPS)³. These weather systems are atmospheric vortices thought to arise from a hydrodynamic
16 instability of the continental-scale monsoon winds that couples with the water vapor field^{4–6}. The vast majority of South Asian
17 LPS form over the northwestern Bay of Bengal then propagate westward, producing intense precipitation as they transit central
18 India to sometimes reach Pakistan and Nepal⁷. LPS also occasionally form over land, the Arabian Sea, and near Sri Lanka⁸.

19 Historical trends in the number of monsoon LPS have been a matter of debate. The stronger LPS—called monsoon
20 depressions—were claimed to have decreased in number by over 50% since the middle of the 20th century^{9–11}. However,
21 the dataset on which those claims were based relied on hand analysis of sea level pressure charts using a set of criteria that
22 seems to have evolved over the decades^{7,12}; no trends in monsoon depression counts were found over the last 40 years in
23 multiple atmospheric reanalyses or in a 25-year satellite scatterometer record of strong surface wind events over the Bay of
24 Bengal^{13,14}. Any observed trends in the number of monsoon depressions may also be confounded by changes in the observing
25 network, such as the incorporation of geostationary satellite data into reanalyses and also into the synoptic analyses of the India

[†]Current affiliation: Météo-France, Direction de la Climatologie et des Services Climatiques, Toulouse, France, and Institute de Recherche pour le Développement (IRD), Nouméa, Nouvelle-Calédonie

26 Meteorological Department starting in the late 1970s and early 1980s¹⁴. However, even if historical trends in the number of
27 monsoon depressions are unclear, other properties of LPS may be changing. In multiple atmospheric reanalyses, LPS tracks
28 exhibit a long-term historical trend of less propagation into northeastern mainland India and more into central and western
29 India, with extreme rainfall shifting along with the storm tracks¹⁵.

30 Given these disparate findings on observed trends in monsoon LPS, it seems worthwhile to ask how LPS respond to
31 anthropogenic forcings in models that reliably simulate these storms. Projections from models that represent all anthropogenic
32 forcings may be particularly important because past trends in Asian precipitation may have been dominated by aerosol
33 forcings, with accompanying uncertainty, while future trends will likely be dominated by greenhouse gas increases^{16–18}. Model
34 representations of internal climate variability are also important, because such variability is evident in historical monsoon
35 depression changes¹⁹ and has been argued to overwhelm the influence of external anthropogenic forcings on Indian monsoon
36 rainfall between 1950 and 2013, with the interdecadal Pacific oscillation playing a central role²⁰. Internal variability also
37 introduces uncertainty in model projections of future monsoon changes²¹. Although models are widely used to project forced
38 and internal monsoon variations, many members of the standard collection of models used to project global climate—assembled
39 in the Coupled Model Intercomparison Project (CMIP)—have been claimed to poorly simulate monsoon LPS, with some of
40 that bias attributed to insufficient horizontal resolution^{3,22}. Finer horizontal resolution in a numerical weather prediction model
41 also generally improved forecasts of LPS track and structure²³. Higher-resolution models have been used to project changes
42 in monsoon LPS, but these have been either (i) individual global models with 0.5°-horizontal grid spacing that have some
43 bias in their representation of LPS and that lack comparison with a model ensemble²⁴, or (ii) regional models with imposed
44 lateral boundary conditions that cannot interact with any changes in the latent heating supplied by the population of LPS²⁵. A
45 lower-resolution model (1° -grid spacing) was found to simulate LPS with realistic intensity and locations in the historical
46 climate, but only represented about half as many systems as observed²⁶; that deficiency, however, may be due to the tracking
47 scheme used in the study, which also identified too few LPS in a reanalysis when compared to track datasets compiled by expert
48 hand analysis⁷.

49 Recently, a tracking algorithm optimized for monsoon LPS was shown to be robust to variations in model horizontal
50 resolution and, when applied to multiple atmospheric reanalyses, to produce results that compare well with hand-analyzed
51 datasets¹⁴. The availability of this algorithm, together with the paucity of analyses of LPS projections in high-resolution global
52 models, motivates the work we present here. Specifically, we analyze the historical and future behavior of monsoon LPS
53 simulated by models participating in the High Resolution Model Intercomparison Project (HighResMIP)²⁷. This avoids reliance
54 on one particular model and leverages the benefits of fine horizontal grid spacing in some of the HighResMIP models (as
55 small as 0.19° longitude × 0.19° latitude), which has been shown to improve simulation of precipitation in the Asian monsoon,
56 perhaps in part because of the high orographic relief of that region²⁸. We identify LPS in this model ensemble using the
57 aforementioned tracking algorithm that was optimized for these storms and is relatively insensitive to the resolution of its input
58 data¹⁴.

59 **2 Results**

60 **2.1 Model skill in capturing observed storms**

61 We first show that HighResMIP models accurately simulate South Asian LPS in the modern climate, and that our tracking
62 algorithm captures not only the easier-to-detect monsoon depressions but also the weaker monsoon lows. When composites of
63 observed and simulated LPS are compared in a vortex-centered reference frame, the models reproduce the cyclonic structure
64 of low-level winds and minima of mean sea level pressure (MSLP) at the storm centers; model intensities are larger than
65 observations, but relative errors in MSLP and in peak 850 hPa horizontal wind speeds are 20% or less in about three-quarters of
66 the models (Fig. 1a, b and Fig. 2f, g). Similar results hold for precipitation, with the ensemble mean having peak rain falling
67 southwest of the vortex center, consistent with observations (Figs. 1c, d and 2c-e). The intensity of the precipitation peak is
68 about 50% larger in models than in observations, with this bias generally increasing as grid spacing decreases, but precipitation
69 averaged horizontally over the storms is within about 20% of observations in most models (Fig. 2d, e). The peak rain also falls
70 closer to the vortex center in the models than in observations; determining why would require understanding the accuracy with
71 which the models simulate dynamical uplift (e.g. quasi-geostrophic lifting), horizontal moisture advection, convective physics,
72 wind-induced ocean evaporation, and the interaction of all of these controls on LPS precipitation²⁹. Overall, these biases are
73 modest, with all eight simulations analyzed here (Table 1) producing generally reasonable structures of winds, precipitation,
74 and MSLP for both lows and depressions (Supplementary Figs. S1, S2).

75 The total number of LPS is also realistic, within about 15% of the observed 15 storms per summer, in all models but the
76 three versions of the HadGEM3 model (Fig. 3a). Distributions of LPS tracks are also realistic, with peak track density over
77 the northwestern Bay of Bengal and central India (Fig. 2a, b); the northward component of storm motion is smaller in the
78 ensemble mean than in observations, which might result from model bias in the structure of the monsoon trough (e.g. its
79 northwest-southeast tilt). The largest bias in track density is again in the HadGEM3 model, which simulates too few storms,
80 especially over the Arabian Sea and western India (Supplementary Fig. S3a-i). Also, the MRI models have a southward bias in
81 their track density. Skill metrics for various quantities, such as storm counts, lifetimes, and intensities, show that biases are
82 heterogeneous across the models (Supplementary Fig. S3j-l stratifies models by skill using metrics using from the CyMeP
83 package³⁰). In general, spatial and temporal correlation coefficients for such quantities, assessed relative to the observed
84 seasonal climatology, range from 0.6 to 0.99, indicating that models simulate comparable spatial distributions and the proper
85 seasonal cycle.

86 It is especially notable that the HighResMIP models successfully simulate monsoon lows, the weaker LPS, with no clear
87 systematic dependence on horizontal resolution (Fig. 1b, d and Supplementary Fig. S1b, S2b). Prior studies detected 40% to
88 70% fewer LPS in coarser-resolution climate models^{26,31} than exist in historical LPS datasets⁷, though this may be partly due
89 to the inability of the tracking algorithms used in those studies to detect weaker systems³². Since even the lowest-resolution
90 version of the Hadley center model simulates the dynamical structure of monsoon lows (Supplementary Figs. S1b and S2b),
91 the good representation of those weaker LPS in our HighResMIP composites might be at least partly due to use of an optimized

92 tracking algorithm that relies on the streamfunction of the horizontal wind instead of the more commonly used (and noisier)
93 vorticity field¹⁴.

94 This ability to detect weaker LPS allows us to examine the partitioning of LPS into lows and depressions, and we find
95 that the models simulate unrealistically large fractions of LPS intensifying to depressions as their horizontal grid spacing
96 decreases. Specifically, in every one of the three models that was run at multiple resolutions, more LPS become depressions at
97 finer horizontal resolutions, with the majority of LPS becoming depressions at the finest resolution (Fig. 3a). This contrasts
98 with reanalyses and historical track datasets⁷, where only about one-third of LPS intensify to depression strength. One might
99 ask if this is due to the tracking algorithm incorrectly classifying more LPS as depressions as the resolution becomes finer,
100 but such bias was not evident when the algorithm was applied to reanalyses¹⁴, nor is it evident in precipitation composited
101 separately for lows and depressions (Supplementary Fig. S2); if the higher number of depressions resulted from an artifact of the
102 tracking algorithm, we would expect depression-related precipitation to weaken at finer model resolutions due to the erroneous
103 categorization of lows as depressions). If this dependence of LPS intensity on model resolution proves to be systematic
104 and general to models, it would be an important deleterious side effect of the move to finer resolution, at least with current
105 parameterization suites.

106 Biases in seasonal-mean summer monsoon rainfall and the strength of the low-level jet (LLJ, i.e. the monsoon westerlies)
107 are assessed to evaluate each model's ability to represent the large-scale monsoon (Fig. 2h). Most models exhibit biases smaller
108 than 20% of the observed values. The HadGEM3 models have the largest rainfall bias with a dry monsoon and a weak LLJ;
109 using finer resolution mitigates these biases in the mean state, but does not result in a clear improvement in LPS representation.
110 Specifically, as the HadGEM3 grid spacing decreases, the bias in LPS-centered rainfall composites decreases (Fig. 2c, d), but
111 the peak LPS rain rates and the radial MSLP gradients become too intense (Fig. 2e, f); the number of LPS remains too low in
112 the HadGEM models as grid spacing is reduced (Fig. 3a).

113 2.2 Trends in storm frequency and location

114 We now examine interdecadal variability and long-term trends in the number of LPS in the HighResMIP models, in both their
115 historical (1950-2014) and future projection (2015 onward) scenarios. Some biases in the models exist, as discussed above, and
116 only two models (the high- and super high-resolution MRI models) have projections extending beyond the year 2050 (Fig. 3a,
117 Table 1). Nevertheless, most of the models simulate realistic counts, locations, and dynamical structures of LPS, and we see
118 multiple common features in the ensemble of projections.

119 The multi-model mean exhibits a decrease in the number of monsoon depressions in the period 1950-2014 (Fig. 3c). The
120 magnitude of this trend is modest, about 0.2 depressions/year/decade (significant when using a 90% confidence interval), when
121 compared with the historical long-term mean value of about 7 depressions/year and also when compared with the roughly 5
122 times larger trend in the subjectively analyzed track record of the India Meteorological Department^{11,13,33}. The HighResMIP
123 multi-model mean trend agrees quantitatively with that in the JRA55 reanalysis, which was only statistically detectable when
124 the season of analysis was expanded by two months to encompass May-October and which was associated with a step-like

125 decrease around the time when that reanalysis began assimilating geostationary satellite data¹⁴. In addition to being present
126 in the multi-model mean, a decrease in depression counts can be seen in 7 out of 8 of the models going from the epoch of
127 1950-1979 to 1980-2009, although the uncertainty associated with this decrease is substantial in some of the models (Fig. 3a).
128 No trends were detected in the number of monsoon lows in the multi-model mean of the historical simulations.

129 In more than half of the models, the simulated historical decrease in the number of monsoon depressions stops or reverses
130 going into the future. This can be seen when comparing different epochs in individual models (e.g. Fig. 3a), and no linear
131 trend is detected in the number of depressions or lows over the period 1980-2050, or the shorter period 2015-2050 (Fig. 3b, c).
132 This changes when one examines the longer-term future projections by the two resolutions of the MRI model, which show
133 a future increase in the number of depressions and a decrease in the lows in projections out to the year 2100. These trends
134 are also modest in magnitude, 0.2-0.4 storms/year/decade compared with long-term mean values of 5-10 storms/year, and the
135 increase in depressions is only marginally statistically significant at the 90th percentile (Fig. 3c). The net result is that the total
136 number of LPS stays constant over the 1950-2100 period in the MRI models. The MRI models simulate more depressions than
137 lows, by a factor of 2 to 1 in the very-high resolution version (Fig. 3a); this bias relative to observations, which have more
138 lows than depressions, reduces confidence in this model's representation of historical and future trends in the partitioning of
139 LPS into lows vs. depressions. One might also have low confidence in the HadGEM3 projections because of that model's poor
140 representation of the seasonal mean state (Fig. 2h) and its deficient number of LPS (Fig. 3a). However, the trends in different
141 periods discussed above change little after excluding the HadGEM3 models from the ensemble mean (Supplementary Fig. S4a,
142 b).

143 Motivated by prior work that found evidence for a shift in LPS locations in observations¹⁵ and in one model's future
144 projections²⁴, we examine trends in LPS genesis and track densities in the HighResMIP ensemble. For the full ensemble,
145 the genesis density of LPS shifts northward going from the historical to the near-future period (1980-2009 to 2020-2049),
146 as indicated by the north-south dipole in the genesis density anomaly over the Bay of Bengal (Fig. 4a). If the HadGEM3
147 models are excluded from this calculation, that dipole has a larger amplitude and is oriented more towards the northwest
148 (Supplementary Fig. S4c) due to the more limited LPS activity in the HadGEM3 models. There is also a shift in genesis density
149 in the end-of-century projections that are available for only the MRI models, but this shift is larger in amplitude and oriented
150 more toward the northwest (Fig. 4b). The changes in genesis density predominantly come from monsoon depressions, with no
151 detectable shift in the genesis density of monsoon lows in the near-future period (Supplementary Fig. S5).

152 These changes are qualitatively consistent with the ocean-to-land shift in LPS genesis found by a prior study of one
153 high-resolution model, explained as being due to the weakening and poleward shift of the low-level monsoon westerlies and
154 the associated background cyclonic vorticity that exists on their northern edge^{24,34}. A weakening and poleward shift of the
155 seasonal-mean low-level monsoon westerlies and the zone of cyclonic vorticity is indeed seen in the HighResMIP ensemble,
156 with anomalous easterlies between the equator and about 12°N and anomalous westerlies near 20-25°N (Fig. 4c, d). In the
157 near-future projections, the poleward shift of the cyclonic vorticity zone is most evident over the Arabian Sea, with a slight

reduction in low-level vorticity over the main genesis region for LPS in the Bay of Bengal. The poleward shift of the seasonal mean cyclonic vorticity zone is more prominent over the Bay of Bengal in the end-of-century projections. Given that enhanced vorticity on the northern side of the low-level monsoon westerlies has been shown to be important for generating monsoon LPS^{4,35}, and given that low-level vorticity has been statistically associated with the frequency of LPS formation³⁶, it seems plausible to accept the poleward shift of the seasonal-mean westerlies as the cause of the changes in genesis seen in the HighResMIP ensemble.

2.3 Rise in storm rain rates

While the ensemble mean shows no detectable change in the number of lows or depressions between recent decades and the year 2050, as discussed above, it exhibits a clear increase in LPS rain rates during that period (Fig. 5a, b), even if the HadGEM3 models are removed from the ensemble mean (Supplementary Fig. S4f, g). The ensemble-mean relative increase in rain rates is about 7% from the historical period to the near future period and about 32% at the end of the 21st century, which is similar to or slightly larger in magnitude than that expected from a Clausius-Clapeyron (CC) scaling with a nominal value of about 7% K⁻¹ (Fig. 5c). Yet, the reasons for this apparently simple scaling of precipitation have some complexity, which we now discuss.

First, there is considerable scatter among individual model projections out to the year 2050, with the normalized relative rates of change of storm-averaged precipitation ranging from nearly zero to about 17% K⁻¹ across the models, each having a substantial uncertainty interval (Fig. 5c). We obtained these relative rates of change by normalizing the fractional change in storm-averaged rain rates by the surface air temperature change averaged over a broad South Asian region (10-25°N, 70-90°E); that region warms consistently across all models by about 1 K in the near-future projections (2020-2049 minus 1980-2009) and about 3 K in the end-of-century projections (2070-2099 minus 1980-2009), so we do not expect the amount of regional warming to be a dominant contributor to inter-model scatter in the rainfall change (Fig. 5d). Further, computing these relative rates of change using temperatures from a larger region (0-30°N and 50-100°E) yields similar results, indicating insensitivity to the specific region. The end-of-century projections from the MRI model exhibit LPS precipitation that increases at about 11% K⁻¹. The very-high-resolution MRI model exhibits almost no change in LPS rain rates in the near-future projection, but a roughly 9% K⁻¹ increase in the extended-future projection (Fig. 5c). Whether this is due to the time evolution of the forcing, internal decadal variability, or some other factor is unclear.

Changes in specific humidity are expected to influence changes in rain rates³⁷, and the low-level specific humidity in LPS increases at a rate of about 6% K⁻¹ to 7% K⁻¹ in six of the eight models, with the other two exhibiting reductions in LPS specific humidity of similar magnitude (Fig. 5c). The weak rate of increase of specific humidity in the multi-model mean of the near-future projections is thus not representative of individual models, most of which scale near the Clausius-Clapeyron rate. The scatter in the rates of change of rainfall thus suggests that dynamical changes accompany the expected warming-induced increase in specific humidity, with some models having LPS rain rates that amplify nearly twice as fast as specific humidity (e.g., the low-resolution version of the HadGEM3 model) while others have rainfall that amplifies more slowly than specific humidity (the high-resolution version of the CNRM model). There is no clear dependence of these inferred dynamical changes

on model resolution, with the caveat that the ensemble is small in size. The end-of-century projections for changes in specific humidity are almost exactly $7\% \text{ K}^{-1}$, indicating some dynamical amplification of rain rates (to about $11\% \text{ K}^{-1}$) in those two projections.

We assess possible changes in the dynamical intensity of LPS by examining the change in the difference of MSLP between the storm center and its surroundings (ΔMSLP ; see Methods). The near-future ensemble-mean change in ΔMSLP is about $4\% \text{ K}^{-1}$ for all LPS, with substantial inter-model scatter, including two models that project a weakening (Fig. 5c). The end-of-century projections exhibit a slightly stronger relative change in ΔMSLP that is consistent between the two resolutions of the MRI model, even though those same two model versions differ in their near-future projections of ΔMSLP (one strengthens, the other weakens). In general, most models project an increase in ΔMSLP , which indicates a strengthening of the dynamical intensity of LPS; this is consistent with the rain rates increasing more rapidly than the specific humidities. There is even consistency in the inter-model scatter of the rain rate changes and the ΔMSLP changes, with the very-high-resolution MRI model exhibiting the largest reduction in ΔMSLP and the lowest rain rate increase in the near-future projections, while the lowest-resolution HadGEM3 model has high values of those two variables. However, it is not appropriate to sum the relative changes in specific humidity and ΔMSLP in an attempt to obtain the rain rate changes, because the rotational winds that are in balance with the radial pressure gradient need not intensify concurrently with the vertical motion field. Indeed, past work has shown that barotropic instability can amplify rotational flow in a vortex without producing strong vertical motion^{38,39}. The changes in rain rates, humidities, and dynamical intensities evaluated for each of the two categories of LPS (lows and depressions) are similar to the changes evaluated for all LPS (Supplementary Fig. S6).

We could be more precise in assessing agreement of these projected rainfall changes with a Clausius-Clapeyron scaling, e.g. by using a more finely tuned set of vertical levels and horizontal regions to assess the humidity and temperature changes. However, it is unclear what three-dimensional region is optimal for assessing warming-induced humidity and temperature changes in LPS⁴⁰. We could instead assume saturated ascent and compute a precipitation change based only on daily vertical motion and temperature change in the individual models⁴¹, but a substantial fraction of LPS precipitation is less intense than that typically used in such scalings for extreme rainfall⁴². Further precision does not seem justified given the large inter-model scatter in changes in humidity, ΔMSLP , and precipitation rates. We show in the next section that shifts in the genesis and tracks of LPS may be as important as any changes in storm rain rates for regional precipitation change.

2.4 LPS contribution to mean and extreme regional rainfall change

The projected increase in LPS rainfall discussed above contributes to projected changes in the seasonal mean and extreme rainfall over South Asia. The ensemble mean exhibits enhanced total summer precipitation and an increased number of extreme precipitation events over nearly all South Asian land, though the changes in these two quantities have differing spatial structures (Fig. 6; we define extreme precipitation as daily events larger than 150 mm in a grid cell). Mean precipitation decreases over the southwest coast of India (Figs. 6a, b); this is on the windward side of the Western Ghats, and is consistent with the poleward shift of the seasonal-mean westerlies discussed above (Fig. 4c, d). A similar reduction in precipitation over this orographic

224 region was seen in an end-of-century projection in another high-resolution model and in observations of the last 100 years^{43,44}.

225 The LPS contribute most strongly to the enhanced mean and extreme precipitation over central India, where in the current
226 climate they produce about half the seasonal mean precipitation and over 80% of the extreme precipitation (Fig. 6). This change
227 is qualitatively similar if we exclude the HadGEM3 models, which have a strong dry bias over central India, from the ensemble
228 mean, albeit with stronger increases over western India (Supplementary Fig. S4d, e). Monsoon depressions and monsoon lows
229 both contribute to the enhanced total and extreme precipitation, with the relative contribution depending on the region and
230 whether the projection is for the near- or extended-future period (Supplementary Fig. S7).

231 The shift in genesis from ocean toward land (discussed above and shown in Fig. 4a, b) is associated with a reduction in the
232 contribution of LPS to mean precipitation over the Bay of Bengal and an increase over central India, especially the western
233 part of central India (Fig. 6a, b). This is reminiscent of the finding that an observed shift in LPS tracks has produced a shift in
234 heavy rainfall over central India over the past 40 years, but that observed shift was southward and confined to land¹⁵, with
235 a pattern highly distinct from the projected northwestward shift found here. The near-future and end-of-century projections
236 exhibit highly similar patterns of change in total precipitation and in the contribution of LPS to that total.

237 Although the models project an increase in the extreme precipitation produced by LPS over central India, there is
238 disagreement as to whether LPS will be responsible for a smaller or larger fraction of the extreme precipitation events. The
239 disagreement primarily results from an increase in this fraction in the HadGEM3 and MRI models, alongside a decrease in the
240 other models. For the near-future projections, fewer than 75% of the models agree on the sign of the change in that contribution
241 (Fig. 6c). The end-of-century projections show an increase in the contribution over central India and a decrease over the Bay of
242 Bengal that resembles the genesis shift, but these projections are from a single model integrated at two different resolutions
243 (Fig. 6d).

244 3 Discussion

245 We have shown that the HighResMIP ensemble skillfully simulates the occurrence frequency, locations, dynamical structures,
246 and rain rates of monsoon LPS, making it a useful tool for projecting future changes in these societally important storms.
247 This contradicts the idea that global model ensemble projections of LPS activity cannot be trusted because of their inadequate
248 skill in simulating LPS. Overall, the HighResMIP ensemble simulated trends in LPS number that are modest in magnitude or
249 undetectable, depending on the multi-decadal period of interest. Over the last half-century in the ensemble mean, the number of
250 depressions decreased by about 1 storm/summer relative to a long-term mean of 7 storms/summer; no historical trend was
251 detected for monsoon lows. In contrast, the ensemble mean showed no linear trend in projected storm counts from the year 2015
252 to the year 2050, or over the combined historical-near future period of 1980-2050. In the one model that projected behavior to
253 2100, the historical decrease in monsoon depression frequency reversed in the future projections and the frequency of lows
254 dropped to keep the total LPS count roughly constant out to the year 2100. Despite the lack of discernible future trends in total
255 LPS counts, the models projected a shift in genesis to the northwest, from ocean toward land, and LPS precipitation rates that

256 increase (around 7% between the historical and near-future periods and around 32% between the historical and extended-future
257 periods). These changes in genesis and rain rates contribute to a projected future increase in seasonal mean and extreme
258 precipitation over South Asian land.

259 These results have some consistency with prior projections made using other models, which can be understood in terms
260 of dynamical changes of the larger-scale monsoon flow. The poleward shift in the genesis distribution resembles that seen
261 in a 0.5° -resolution atmospheric model forced with an ensemble of end-of-century SST projections²⁴. That model, however,
262 also simulated a decline in the total number of LPS that was not seen in the HighResMIP ensemble; its historical simulations
263 were additionally biased by simulating LPS that were too intense, although of the same number as observed. Another study
264 also found a decrease in the total number of LPS of about 15%, but with no poleward shift, in end-of-century projections by a
265 1° -resolution coupled ocean-atmosphere model²⁶; the number of LPS in that model's historical climate was about half of the
266 observed number, although this may be due to the tracking scheme used in that study which also identified too few LPS in a
267 reanalysis. Both of those studies argued that the reduction in LPS genesis results from a weakening of the large-scale, low-level
268 monsoon westerlies and a corresponding reduction in vorticity over the northern Bay of Bengal and South Asia^{24,26}. An earlier
269 analysis of a 2° -resolution coupled model found no change in the number of monsoon depressions in response to a quadrupling
270 of CO₂, but then downscaled the results using a 0.75° -resolution regional model (with imposed lateral boundary conditions) to
271 find that the stronger LPS increased in number⁴⁵; the region of genesis over the Bay of Bengal also shifted poleward in that
272 study's 2° global model and its regional downscaling, together with the seasonal-mean low-level westerlies.

273 Other studies have examined projections of LPS in the coarser-resolution CMIP ensemble, but the combination of tracking
274 algorithms and models used makes those difficult to interpret in the context of our results. One study found no change in the
275 number of South Asian LPS in end-of-century projections, but used a tracking algorithm that identified only about six LPS
276 per year in models and reanalyses³¹, compared with double that found by our tracking algorithm¹⁴ and in a hand-analyzed
277 expert dataset⁷. Structures of the LPS were not examined in that study³¹. All of this demonstrates the importance of using an
278 optimized tracking algorithm in conjunction with models that have been well validated to represent both categories of LPS, as
279 was done here.

280 The weak reduction in the number of monsoon depressions seen in the historical simulations and the absence of any such
281 reduction in the near- and extended-future projections are important results. These results contrast with the roughly 5 times
282 larger reduction in the number of depressions seen between the 1970s and early 2000s in India Meteorological Department
283 records^{9–11}. The HighResMIP trends are instead quantitatively consistent with the weak trend found in one reanalysis during
284 the period 1958–2019, and with the absence of any detectable trend in 4 other reanalyses for the later period of 1979–2019¹⁴.
285 Altogether, this model ensemble provides an additional reason to expect the population of South Asian monsoon LPS to remain
286 roughly constant in number while shifting poleward and producing more intense precipitation in coming decades.

287 **4 Methods**

288 **4.1 High-resolution model ensemble**

289 All simulations used here employed the Coupled Model Intercomparison Project Phase 6 (CMIP6) HighResMIP experimental
290 design²⁷. The climate of recent decades is obtained from the HighResMIP Tier 1 experiment, a historical (1950–2014)
291 atmosphere-only configuration that uses observed HadISST2 sea surface temperatures (SSTs) as a lower boundary condition
292 with prescribed historical changes in greenhouse gas concentrations, aerosols, and natural radiative forcings due to volcanism
293 and solar variability⁴⁶. Since monsoon LPS have weak surface winds and spend a short amount of time over ocean, we do not
294 expect the use of prescribed SST to greatly alter their individual short-term evolution, but use of prescribed SST may introduce
295 bias into the projections of the seasonal mean monsoon circulation in which they are embedded.

296 Future projections are obtained from HighResMIP Tier 3, which is also an atmosphere-only configuration but with an SST
297 boundary condition that blends interannual variability from the HadISST2 SST dataset with a climate change signal from
298 CMIP5 RCP8.5 models; these simulations obtained greenhouse gas forcings from the CMIP6 SSP585 scenario, and used a
299 simplified representation of anthropogenic aerosol changes consistent with that high-end emissions scenario^{27,47}. Using a
300 high-emissions scenario such as SSP585 is appropriate for this study, even if such a scenario is not the most likely one to
301 occur in the future, because of the large scientific uncertainty in the sign of the response of LPS to anthropogenic forcings
302 (as discussed in the Introduction). That is, we use a large forcing to determine if this can produce any detectable change in
303 LPS counts, locations, and other properties. The future projection simulations begin in the year 2015, with most models
304 simulating to 2050 and a few to 2100.

305 We used a total of eight model runs, consisting of simulations performed at multiple resolutions using models from four
306 different institutes (Table 1). The availability of simulations conducted at multiple resolutions for some of these models allows
307 for assessment, albeit with small sample size, of the influence of model resolution on LPS behavior.

Table 1. Details of HighResMIP models used in this study.

| Model | Version | Acronym | Future period | Resolution | Source |
|---------------|-----------|---------|---------------|---------------------------------|---|
| CNRM-CM6 | Low | CNRM | 2015-2050 | $1.41^\circ \times 1.40^\circ$ | CERFACS, France ⁴⁸ |
| | High | CNRM-H | 2015-2050 | $0.5^\circ \times 0.5^\circ$ | |
| MRI-AGCM3-2 | High | MRI-H | 2015-2100 | $0.56^\circ \times 0.56^\circ$ | MRI, Japan ⁴⁹ |
| | Very High | MRI-S | 2015-2100 | $0.19^\circ \times 0.19^\circ$ | |
| HadGEM3-GC3.1 | Low | Had-L | 2015-2050 | $1.875^\circ \times 1.25^\circ$ | Met Office Hadley Centre, UK ⁵⁰ |
| | High | Had-M | 2015-2050 | $0.83^\circ \times 0.56^\circ$ | |
| | Very High | Had-H | 2015-2050 | $0.35^\circ \times 0.23^\circ$ | |
| EC-Earth3P | High | EC-3P | 2015-2050 | $0.70^\circ \times 0.70^\circ$ | EC-Earth consortium ⁵¹ |

308 We use monthly and six-hourly HighResMIP precipitation and pressure-level values of horizontal wind, specific humidity,
309 and air temperature. We choose the years 1980-2009 as the reference period of the historical simulations, and compare these
310 with a near future (Nfut) period spanning 2020-2049 and an extended future (Efut) period spanning 2070-2099.

311 **4.2 Observational data**

312 We compare output from the HighResMIP simulations with multiple observational and reanalysis products. We use precipitation
313 data from the Tropical Rainfall Measurement Mission (TRMM)⁵² and the India Meteorological Department (IMD) gauge-based
314 datasets⁵³. We obtain mean sea level pressure (MSLP) and horizontal wind from ERA5, the fifth generation atmospheric
315 reanalysis from the European center for Medium-Range Weather Forecasts (ECMWF)⁵⁴.

316 Observed LPS tracks for 1979-2019 are obtained from the prior application of a tracking algorithm optimized for monsoon
317 LPS to multiple atmospheric reanalyses, with the track datasets available as a Zenodo archive⁵⁵.

318 **4.3 Tracking and analysis methods**

319 The tracking algorithm is based on the TempestExtremes framework⁵⁶, with the variables and thresholds used for tracking
320 selected from hundreds of combinations based on the level of agreement between multiple atmospheric reanalyses and an
321 expert-derived, hand-analyzed dataset¹⁴. The selected algorithm uses the streamfunction of the horizontal 850 hPa wind, which
322 is smoother than the more commonly used vorticity field and does not make the balance assumptions required when tracking is
323 based on MSLP. More details are in the original study that details the algorithm and its success¹⁴.

324 The chosen tracking algorithm employed the 850 hPa streamfunction minima, which we required to increase by 1.25×10^6
325 from the central minimum within a 10° radius to identify vortices. For differentiation from heat lows, the algorithm required an
326 850 hPa relative humidity of at least 85% for a continuous period of at least one day along the track. Successive points were
327 linked by ensuring that candidate points fell within 3° of each other over 12 hours.

328 We use the same tracking algorithm to characterize LPS in the HighResMIP models and reanalyses, obtaining genesis
329 points and tracks, and categorizing LPS as monsoon lows (weaker LPS) or monsoon depressions (MDs; stronger LPS) based on
330 their intensities. Specifically, lows have surface wind speeds less than 8.5 m s^{-1} and central MSLP at least 2 hPa lower than
331 surrounding regions, while MDs have wind speeds of at least 8.5 m s^{-1} and MSLP at least 4 hPa lower than the surroundings⁵⁷.
332 Stronger vortices called cyclonic storms are improbable but possible in the South Asian summer monsoon period, so we
333 consider MD as MD and above intensities.

334 We produce storm-centered composites of several variables by averaging over time along each LPS track in a latitude-
335 longitude coordinate system centered on the streamfunction minimum (irrespective of the LPS propagation direction), then
336 averaging over all storms. This results in each storm having the same weight in the composite, regardless of its duration. Some
337 variables, such as precipitation and humidity, are also averaged horizontally over a circle of radius 3° around the vortex center.
338 The monsoon low and depression composites are time-averages of all time steps during which an LPS had that intensity; since
339 depressions generally originate first as lows, this ensures that the time a vortex spends as a low does not contribute to the
340 composites of depressions. The composites for lows and depressions are thus based on the instantaneous storm intensity rather
341 than on the peak intensity achieved along a storm track. The dynamical intensity of LPS is assessed by estimating the radial
342 change in MSLP between the minimum MSLP near the vortex center and the storm surroundings. We refer to this quantity as
343 ΔMSLP , and it is obtained from the tracking algorithm^{14,56}.

344 Model biases are calculated for different variables (Fig. 2) as the percentage difference between modeled and observed
345 values. Track density is computed using kernel density estimation of cumulative track points over the specified period. All
346 linear trends were calculated using the Python 'statsmodels' module⁵⁸. Two-tailed p-values were obtained from the t-statistics
347 of the linear model parameters.

348 **Data Availability**

349 The monsoon low-pressure system track data for reanalyses was obtained from the Zenodo archive (<https://zenodo.org/record/3890646#.ZAmsIi9U1QI>). The ERA5 data set was obtained from the Copernicus Climate Change
350 Service Climate Data Store (CDS) website (at <https://cds.climate.copernicus.eu/cdsapp#/home>), ac-
351 cessed on 1 March 2021. Tropical Rainfall Measuring Mission (TRMM) daily precipitation data was downloaded from
352 the NASA GSFC website (https://disc.gsfc.nasa.gov/datasets/TRMM_3B42_Daily_7/summary). The
353 HighResMIP model data was downloaded from The Earth System Grid Federation infrastructure (ESGF) archive (<https://esgf-node.llnl.gov/search/cmip6/tipl>). All data used in the paper are acknowledged in the Methods section.
355

356 **Code Availability**

357 Code to produce the figures is available from the corresponding author on request.

358 **Additional information**

359 **Competing interests** (The authors declare no competing interests.).

360 **Acknowledgments**

361 This material is based upon work supported by the U.S. Department of Energy, Office of Science, Office of Biological
362 and Environmental Research, Climate and Environmental Sciences Division, Regional & Global Model Analysis (RGMA)
363 Program, under Award Numbers DE-AC02-05CH11231 and DE-SC0019367. WRB and WDC were supported under RGMA's
364 Calibrated and Systematic Characterization, Attribution, and Detection of Extremes (CASCADE) Scientific Focus Area.
365 This research used resources of the National Energy Research Scientific Computing Center (NERSC), a U.S. Department
366 of Energy Office of Science User Facility located at Lawrence Berkeley National Laboratory, operated under Contract No.
367 DE-AC02-05CH11231 using NERSC awards BER-ERCAPm1517 and BER-ERCAPm3310. The authors also acknowledge
368 support from the Earth System Science Organization, Ministry of Earth Sciences, Government of India (Grant IITM/MM-II/
369 Univ_California_USA/INT-3) under the Monsoon Mission.

370 We acknowledge the World Climate Research Programme, which, through its Working Group on Coupled Modelling,
371 coordinated and promoted CMIP6. We thank the climate modeling groups for producing and making available their model
372 output, the Earth System Grid Federation (ESGF) for archiving the data and providing access, and the multiple funding agencies
373 who support CMIP6 and ESGF.

374 The authors thank the modeling groups within PRIMAVERA (a European Union Horizon 2020 project under Grant
375 Agreement 641727) for producing the multi-model simulations and providing the climate model outputs via the Earth System
376 Grid Federation (ESGF). The authors greatly appreciate Malcolm Roberts and Jon Seddon (UK Met Office Hadley Centre) for
377 their help in accessing the model data through the UK Centre for Environmental Data Analysis's JASMIN platform.

378 **Author Contributions**

379 S.V. and W.R.B. conceived the research, analyzed data, and wrote the manuscript. W.D.C. performed early data analysis and
380 supported the use of the HighResMIP data. All authors read and edited the manuscript.

381 **References**

- 382 1. Roxy, M. K. *et al.* A threefold rise in widespread extreme rain events over central India. *Nat. communications* **8**, 1–11
383 (2017).
- 384 2. Vishnu, S., Risser, M. D., O'Brien, T. A., Ullrich, P. A. & Boos, W. R. Observed increase in the peak rain rates of monsoon
385 depressions. *npj Clim. Atmospheric Sci.* **6**, 111 (2023).
- 386 3. Praveen, V., Sandeep, S. & Ajayamohan, R. On the relationship between mean monsoon precipitation and low pressure
387 systems in climate model simulations. *J. Clim.* **28**, 5305–5324 (2015).
- 388 4. Diaz, M. & Boos, W. R. Barotropic growth of monsoon depressions. *Q. J. Royal Meteorol. Soc.* DOI: [10.1002/qj.3467](https://doi.org/10.1002/qj.3467)
389 (2019).
- 390 5. Adames, Á. F. & Ming, Y. Interactions between water vapor and potential vorticity in synoptic-scale monsoonal
391 disturbances: Moisture vortex instability. *J. Atmospheric Sci.* **75**, 2083–2106 (2018).
- 392 6. Diaz, M. & Boos, W. R. The Influence of Surface Heat Fluxes on the Growth of Idealized Monsoon Depressions. *J.
393 Atmospheric Sci.* **78**, 2013–2027, DOI: [10.1175/JAS-D-20-0359.1](https://doi.org/10.1175/JAS-D-20-0359.1) (2021).
- 394 7. Sikka, D. *A study on the monsoon low pressure systems over the Indian region and their relationship with drought and
395 excess monsoon seasonal rainfall* (Center for Ocean-Land-Atmosphere Studies, Center for the Application of Research on
396 the Environment, 2006).
- 397 8. Deoras, A., Hunt, K. M. & Turner, A. G. The four regional varieties of south asian monsoon low-pressure systems and
398 their modulation by tropical intraseasonal variability. *Weather* **76**, 194–200 (2021).
- 399 9. Dash, S. K., Kumar, J. J. R. & Shekhar, M. S. M. On the decreasing frequency of monsoon depressions over the Indian
400 region. *Curr. Sci.* **86**, 1404–1411 (2004).
- 401 10. Dash, S. K., Jenamani, R. K., Kalsi, S. R. & Panda, S. K. Some evidence of climate change in twentieth-century India.
402 *Clim. Chang.* **85**, 299–321, DOI: [10.1007/s10584-007-9305-9](https://doi.org/10.1007/s10584-007-9305-9) (2007).

- 403 11. Vishnu, S., Francis, P., Shenoi, S. & Ramakrishna, S. On the decreasing trend of the number of monsoon depressions in the
404 Bay of Bengal. *Environ. Res. Lett.* **11**, 014011 (2016).
- 405 12. Mooley, D. & Shukla, J. *Characteristics of the westward-moving summer monsoon low pressure systems over the Indian*
406 *region and their relationship with the monsoon rainfall* (University of Maryland, Department of Meteorology, Center for
407 Ocean-Land-Atmosphere Interactions, 1987).
- 408 13. Cohen, N. Y. & Boos, W. R. Has the number of Indian summer monsoon depressions decreased over the last 30 years?
409 *Geophys. Res. Lett.* **41**, 7846–7853 (2014).
- 410 14. Vishnu, S., Boos, W. R., Ullrich, P. A. & O'Brien, T. A. Assessing Historical Variability of South Asian Monsoon Lows
411 and Depressions With an Optimized Tracking Algorithm. *J. Geophys. Res. Atmospheres* **125**, e2020JD032977, DOI:
412 [10.1029/2020JD032977](https://doi.org/10.1029/2020JD032977) (2020).
- 413 15. You, Y. & Ting, M. Observed trends in the South Asian monsoon low-pressure systems and rainfall extremes since the late
414 1970s. *Geophys. Res. Lett.* **48**, e2021GL092378 (2021).
- 415 16. Lau, W. K.-M. & Kim, K.-M. Competing influences of greenhouse warming and aerosols on Asian summer monsoon
416 circulation and rainfall. *Asia-Pacific J. Atmospheric Sci.* **53**, 181–194 (2017).
- 417 17. Cao, J. *et al.* Higher sensitivity of northern hemisphere monsoon to anthropogenic aerosol than greenhouse gases. *Geophys.*
418 *Res. Lett.* **49**, e2022GL100270 (2022).
- 419 18. Arias, P. *et al.* *Technical Summary; Climate Change 2021: The Physical Science Basis. Contribution of Working Group I to*
420 *the Sixth Assessment Report of the Intergovernmental Panel on Climate Change* (Cambridge University Press, Cambridge,
421 United Kingdom and New York, NY, USA, 2021).
- 422 19. Vishnu, S., Francis, P. A., Shenoi, S. C. & Ramakrishna, S. S. V. S. On the relationship between the pacific decadal
423 oscillation and monsoon depressions over the bay of bengal. *Atmospheric Sci. Lett.* **19**, e825 (2018).
- 424 20. Huang, X. *et al.* The recent decline and recovery of indian summer monsoon rainfall: relative roles of external forcing and
425 internal variability. *J. Clim.* **33**, 5035–5060 (2020).
- 426 21. Huang, X. *et al.* South asian summer monsoon projections constrained by the interdecadal pacific oscillation. *Sci. advances*
427 **6**, eaay6546 (2020).
- 428 22. Ashfaq, M., Rastogi, D., Mei, R., Touma, D. & Ruby Leung, L. Sources of errors in the simulation of south Asian summer
429 monsoon in the CMIP5 GCMs. *Clim. Dyn.* **49**, 193–223 (2017).
- 430 23. Hunt, K. M. & Turner, A. G. The effect of horizontal resolution on indian monsoon depressions in the met office nwp
431 model. *Q. J. Royal Meteorol. Soc.* **143**, 1756–1771 (2017).
- 432 24. Sandeep, S., Ajayamohan, R., Boos, W. R., Sabin, T. & Praveen, V. Decline and poleward shift in Indian summer monsoon
433 synoptic activity in a warming climate. *Proc. Natl. Acad. Sci.* **115**, 2681–2686 (2018).

- 434 25. Sørland, S. L., Sorteberg, A., Liu, C. & Rasmussen, R. Precipitation response of monsoon low-pressure systems to an
435 idealized uniform temperature increase. *J. Geophys. Res. Atmospheres* **121**, 6258–6272 (2016).
- 436 26. Dong, W., Ming, Y. & Ramaswamy, V. Projected changes in South Asian monsoon low pressure systems. *J. Clim.* **33**,
437 7275–7287 (2020).
- 438 27. Haarsma, R. J. *et al.* High resolution model intercomparison project (HighResMIP v1. 0) for CMIP6. *Geosci. Model. Dev.*
439 **9**, 4185–4208 (2016).
- 440 28. Delworth, T. L. *et al.* Simulated climate and climate change in the GFDL CM2.5 high-resolution coupled climate model. *J.*
441 *Clim.* **25**, 2755–2781, DOI: [10.1175/JCLI-D-11-00316.1](https://doi.org/10.1175/JCLI-D-11-00316.1) (2012).
- 442 29. Murthy, V. S. & Boos, W. R. Quasigeostrophic controls on precipitating ascent in monsoon depressions. *J. Atmospheric*
443 *Sci.* **77**, 1213–1232 (2020).
- 444 30. Zarzycki, C. M., Ullrich, P. A. & Reed, K. A. Metrics for evaluating tropical cyclones in climate data. *J. Appl. Meteorol.*
445 *Climatol.* **60**, 643–660 (2021).
- 446 31. Rastogi, D. *et al.* Characteristics of Bay of Bengal monsoon depressions in the 21st century. *Geophys. Res. Lett.* **45**,
447 6637–6645 (2018).
- 448 32. Srujan, K. S., Sandeep, S. & Suhas, E. Downstream and in situ genesis of monsoon low-pressure systems in climate
449 models. *Earth Space Sci.* **8**, e2021EA001741 (2021).
- 450 33. Prajesh, A., Ashok, K. & Rao, D. B. Falling monsoon depression frequency: A Gray-Sikka conditions perspective. *Sci.*
451 *Reports* **3**, 2989 (2013).
- 452 34. Sandeep, S. & Ajayamohan, R. Poleward shift in Indian summer monsoon low level jetstream under global warming. *Clim.*
453 *Dyn.* **45**, 337–351 (2015).
- 454 35. Nitta, T. & Masuda, K. Observational Study of a Monsoon Depression Developed Over the Bay of Bengal during Summer
455 MONEX. *J. Meteorol. Soc. Jpn. Ser. II* **59**, 672–682 (1981).
- 456 36. Ditcheck, S., Boos, W., Camargo, S. & Tippett, M. A genesis index for monsoon disturbances. *J. Clim.* **29**, 5189–5208,
457 DOI: [10.1175/JCLI-D-15-0704.1](https://doi.org/10.1175/JCLI-D-15-0704.1) (2016).
- 458 37. Allen, M. R. & Ingram, W. J. Constraints on future changes in climate and the hydrologic cycle. *Nature* **419**, 224–232
459 (2002).
- 460 38. Suhas, D. & Boos, W. R. Monsoon depression amplification by horizontal shear and humidity gradients: a shallow water
461 perspective. *J. Atmospheric Sci.* **80**, 633–647 (2023).
- 462 39. Diaz, M. & Boos, W. R. Monsoon depression amplification by moist barotropic instability in a vertically sheared
463 environment. *Q. J. Royal Meteorol. Soc.* **145**, 2666–2684 (2019).

- 464 40. Diaz, M. & Boos, W. R. Evolution of idealized vortices in monsoon-like shears: Application to monsoon depressions. *J.*
465 *Atmospheric Sci.* **78**, 1207–1225 (2021).
- 466 41. O’Gorman, P. A. & Schneider, T. The physical basis for increases in precipitation extremes in simulations of 21st-century
467 climate change. *Proc. Natl. Acad. Sci.* **106**, 14773–14777 (2009).
- 468 42. Pfahl, S., O’Gorman, P. A. & Fischer, E. M. Understanding the regional pattern of projected future changes in extreme
469 precipitation. *Nat. Clim. Chang.* **7**, 423–427 (2017).
- 470 43. Rajendran, K., Kitoh, A., Srinivasan, J., Mizuta, R. & Krishnan, R. Monsoon circulation interaction with Western Ghats
471 orography under changing climate: projection by a 20-km mesh AGCM. *Theor. Appl. Climatol.* **110**, 555–571 (2012).
- 472 44. Caretta, M. A. *et al.* Water. In: Climate Change 2022: Impacts, Adaptation, and Vulnerability. Contribution of Working
473 Group II to the Sixth Assessment Report of the Intergovernmental Panel on Climate Change (2022).
- 474 45. Stowasser, M., Annamalai, H. & Hafner, J. Response of the South Asian summer monsoon to global warming: Mean and
475 synoptic systems. *J. Clim.* **22**, 1014–1036 (2009).
- 476 46. Kennedy. The Met Office Hadley Centre Sea Ice and Sea-Surface Temperature data set, version 2.2.0.0 (2018).
- 477 47. Stevens, B. *et al.* Macv2-sp: A parameterization of anthropogenic aerosol optical properties and an associated twomey
478 effect for use in cmip6. *Geosci. Model. Dev.* **10**, 433–452 (2017).
- 479 48. Volodire, A. *et al.* Evaluation of CMIP6 deck experiments with CNRM-CM6-1. *J. Adv. Model. Earth Syst.* **11**, 2177–2213
480 (2019).
- 481 49. MIZUTA, R. *et al.* Climate Simulations Using MRI-AGCM3.2 with 20-km Grid. *J. Meteorol. Soc. Jpn. Ser. II* **90A**,
482 233–258, DOI: [10.2151/jmsj.2012-A12](https://doi.org/10.2151/jmsj.2012-A12) (2012).
- 483 50. Roberts, M. J. *et al.* Description of the resolution hierarchy of the global coupled HadGEM3-GC3. 1 model as used in
484 CMIP6 HighResMIP experiments. *Geosci. Model. Dev.* **12**, 4999–5028 (2019).
- 485 51. Haarsma, R. *et al.* HighResMIP versions of EC-Earth: EC-Earth3P and EC-Earth3P-HR—description, model computational
486 performance and basic validation. *Geosci. Model. Dev.* **13**, 3507–3527 (2020).
- 487 52. Huffman, G. J. *et al.* The TRMM multisatellite precipitation analysis (TMPA): Quasi-global, multiyear, combined-sensor
488 precipitation estimates at fine scales. *J. hydrometeorology* **8**, 38–55 (2007).
- 489 53. Pai, D. *et al.* Development of a new high spatial resolution (0.25×0.25) long period (1901–2010) daily gridded rainfall
490 data set over India and its comparison with existing data sets over the region. *Mausam* **65**, 1–18 (2014).
- 491 54. Hersbach, H. *et al.* The era5 global reanalysis. *Q. J. Royal Meteorol. Soc.* **146**, 1999–2049 (2020).
- 492 55. Vishnu, S., Boos, W. R., Ullrich, P. A. & O’Brien, T. A. Global track dataset of monsoon low pressure systems. *Zenodo*
493 <https://doi.org/10.5281/zenodo.3890646> (2020).

- 494 56. Ullrich, P. A. & Zarzycki, C. M. TempestExtremes: A framework for scale-insensitive pointwise feature tracking on
 495 unstructured grids. *Geosci. Model. Dev.* **10**, 1069 (2017).
- 496 57. India Meteorological Department. *Tracks of cyclones and depressions over North Indian Ocean (from 1891 onwards)*,
 497 *Tech. Note Version 2.0* (Cyclone Warning and Research Centre India Meteorological Department Regional Meteorological
 498 Centre, Chennai, India, 2011).
- 499 58. Seabold, S. & Perktold, J. statsmodels: Econometric and statistical modeling with python. In *9th Python in Science*
 500 *Conference* (2010).

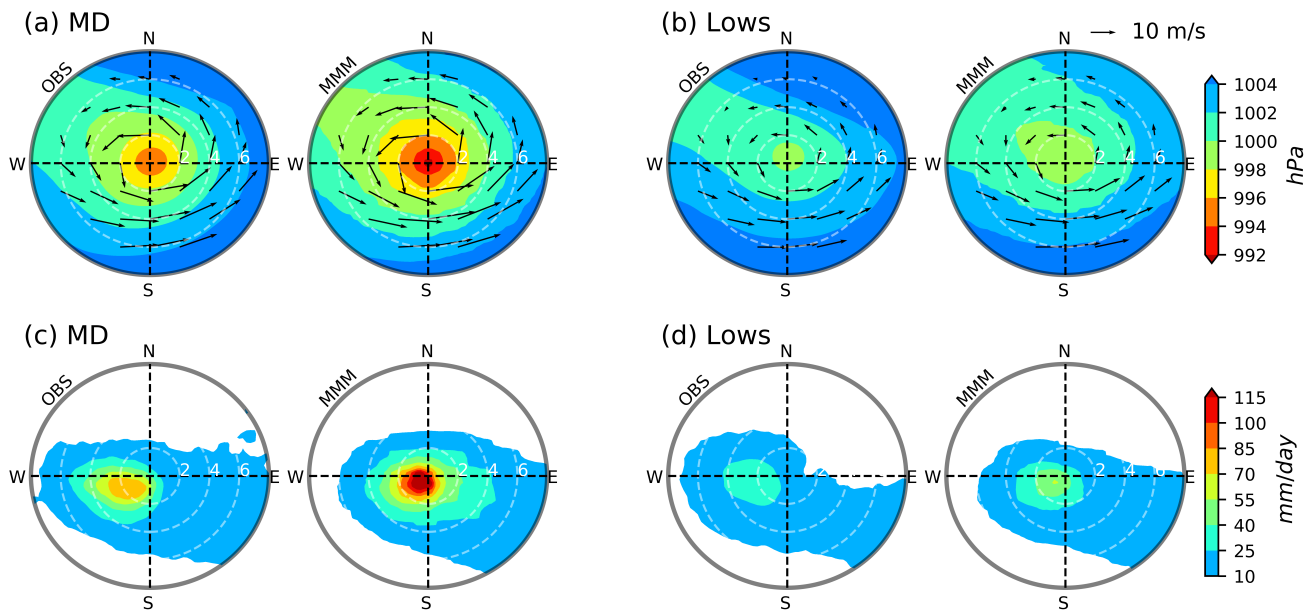


Figure 1. Model representation of monsoon low pressure system structure. Vortex-centered composites of mean sea level pressure (MSLP, shaded) and horizontal wind at 850 hPa (vectors) in observations (left) and the multi-model mean (right) for (a) monsoon depressions (MD) and (b) monsoon lows. Panels (c) and (d) are the same as (a) and (b) but for precipitation. Models contributing to the multi-model mean are listed in Table 1, ERA5 data is used as the estimate of observed MSLP and horizontal wind, and TRMM data is used as the estimate of precipitation. Wind and MSLP were composited for years 1980–2009 (the historical model period) and precipitation for 1998–2013 (a period that allows comparison with TRMM observations).

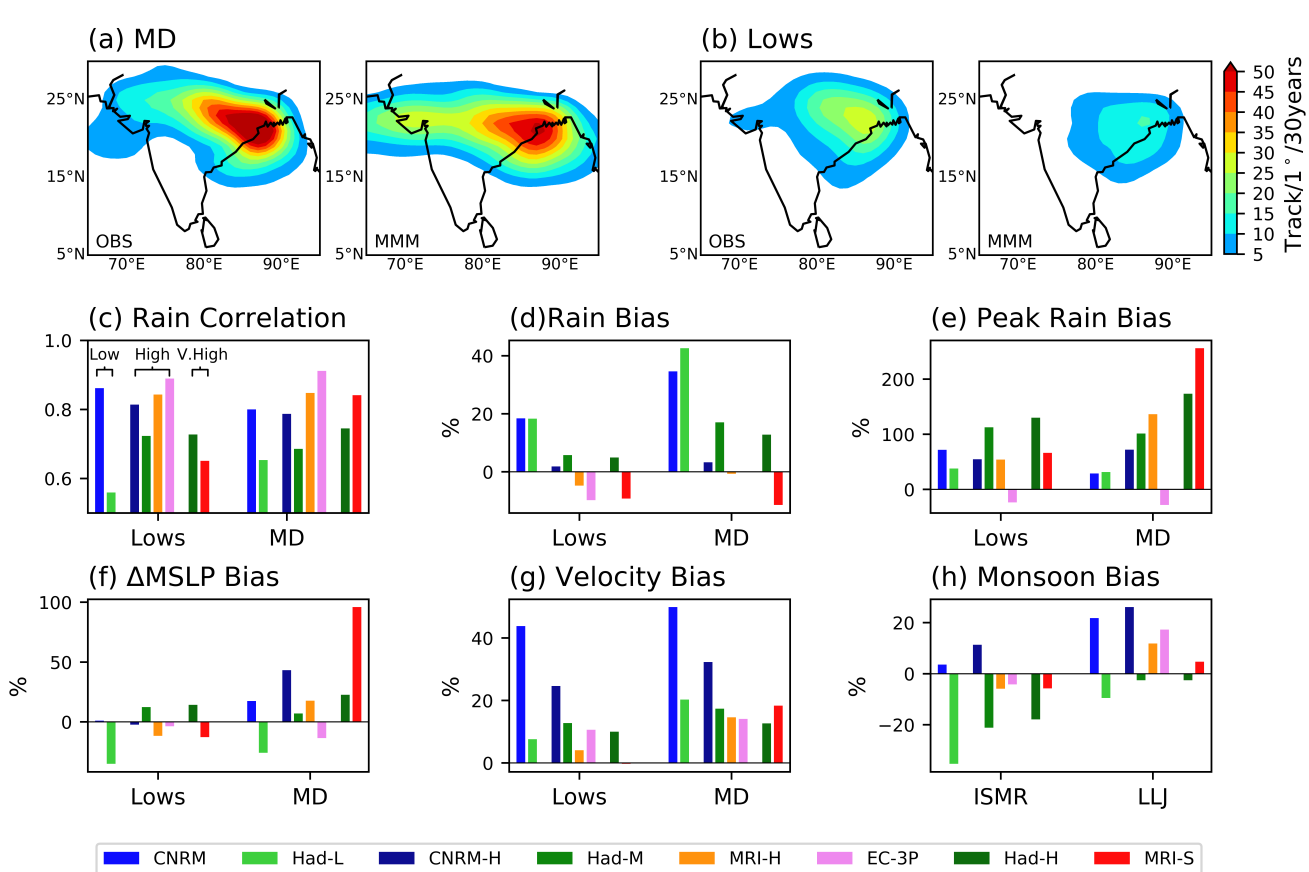


Figure 2. Model skill in capturing low pressure system tracks and intensities. Track density of (a) monsoon depressions (MD) and (b) monsoon lows for 1980–2009 in observations (left) and the multi-model mean (right). Skill metrics for each model's representation of several parameters of lows and monsoon depressions, specifically (c) the pattern correlation coefficient of vortex-centered composite precipitation, (d) model bias in precipitation averaged within 3° of the vortex center, (e) model bias in peak precipitation, (f) model bias in ΔMSLP , the magnitude of the radial change in the vortex-centered composite of MSLP between the surroundings and the storm minimum value, and (g) model bias in the 850 hPa spatial maximum wind speed within 3° of vortex center in the vortex-centered composite. (h) Bias in seasonal total Indian summer monsoon rainfall (ISMR; left) and strength of the westerly low-level jet (LLJ; right). ISMR is the June–September rainfall averaged $10\text{--}30^\circ\text{N}$ and $70\text{--}100^\circ\text{E}$, and the LLJ strength is the latitudinal maximum of zonal wind averaged over $60\text{--}90^\circ\text{E}$ at 850 hPa. All biases and correlations are computed relative to TRMM precipitation and ERA5 winds and MSLP. Models are grouped based on the resolution category (see panel c) and are listed in Table 1.

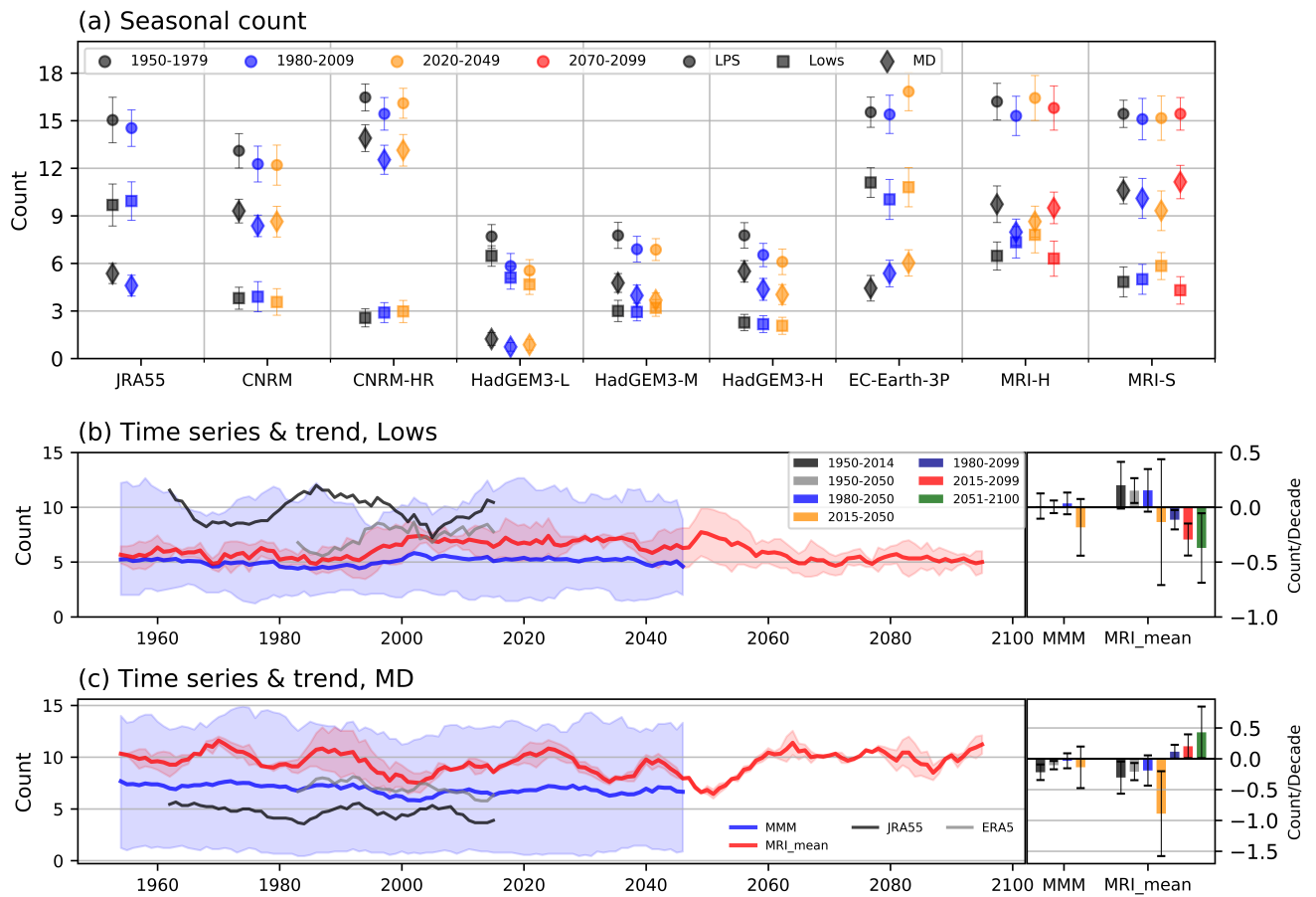


Figure 3. Decadal variability and long-term trends in storm counts. (a) Seasonal number of all LPS (circles), monsoon lows (squares) and monsoon depressions (diamonds) in various 30-year periods. Time series and trends of the number of (b) monsoon lows and (c) monsoon depressions (time series are 9-year running means). In the left panels of (b) and (c), thick red and blue lines represent the multi-model means of the models having, respectively, extended-future projections to 2100 (the MRI-H and MRI-S models, MRI_mean) and near-future projections to 2050 (the full 8-member ensemble, MMM). Shading shows the spread across the models, and the thin black and gray lines show the JRA55 and ERA5 reanalyses (JRA55 is included due to its availability before the year 1979). The right panels of (b) and (c) show linear trends in storm counts over different periods denoted in the legend. The error bars in (a)-(c) represent a 90% confidence interval.

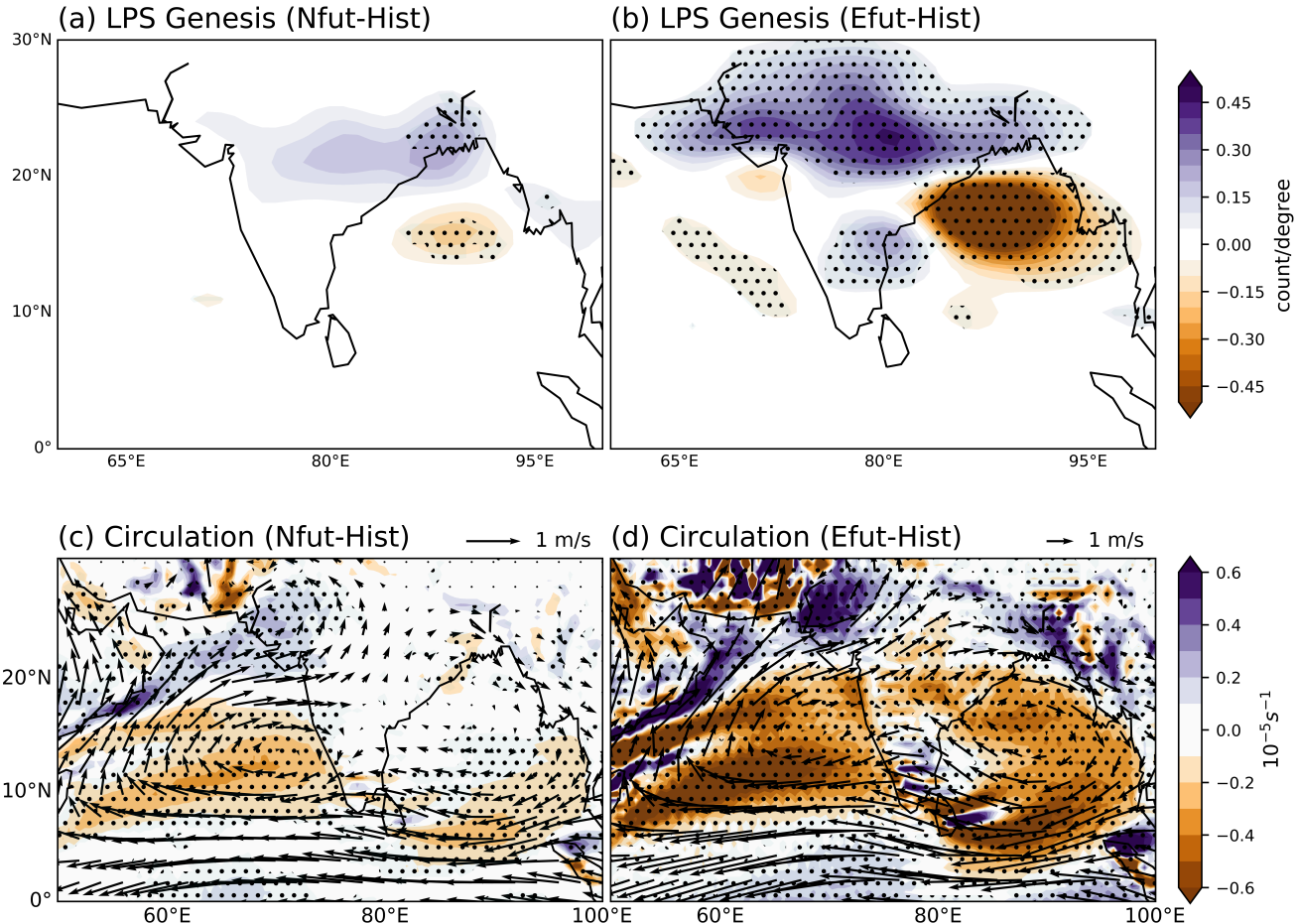


Figure 4. Change in the LPS genesis distribution and the large-scale, low-level westerlies. Multi-model mean changes in the genesis density of all LPS (a) from the historical period (1980-2009) to the near future period (2020-2049), and (b) from the historical period to the end of the 21st century (2070-2099). Shading shows the change in the number of LPS genesis points per square-degree per summer. Panels (c) and (d) are the same as (a) and (b) but for the seasonal-mean relative vorticity (shaded) and horizontal wind at 850 hPa (vectors). Stippling shows regions where at least 75% of the model simulations have the same sign of change.

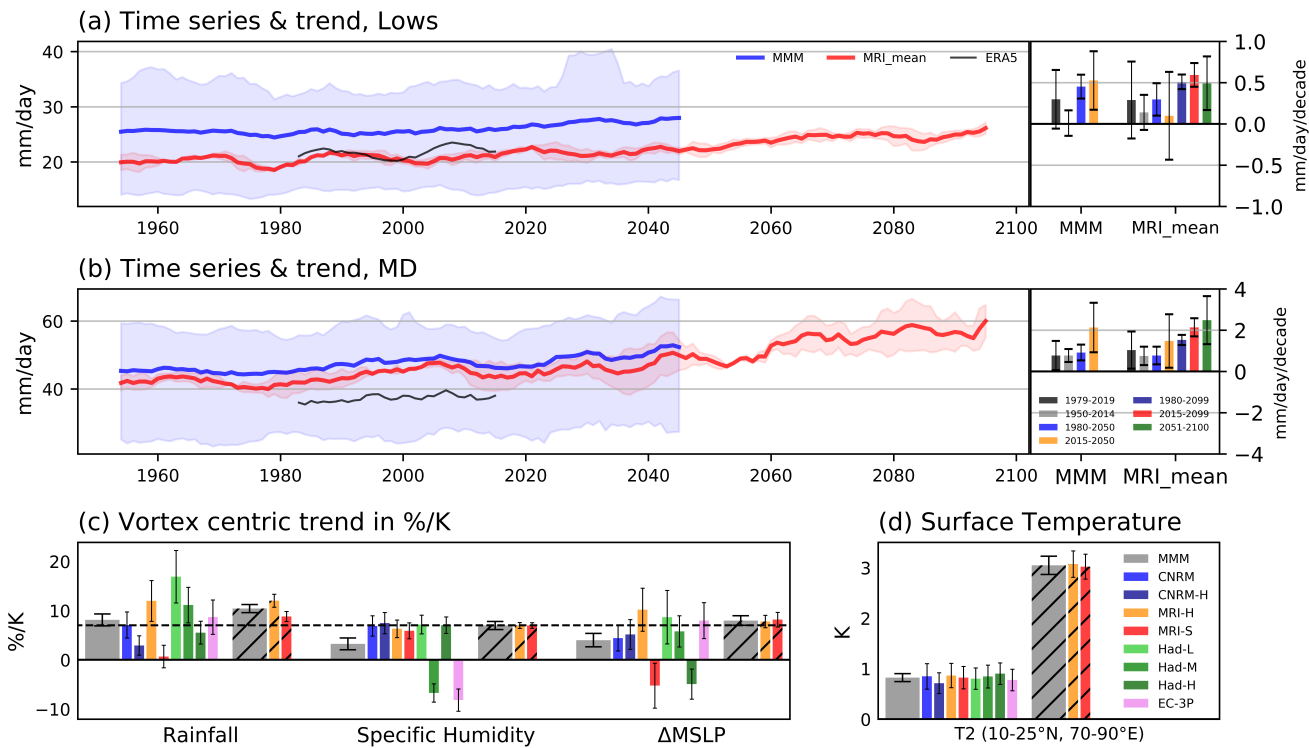


Figure 5. Decadal variability and long-term trends in LPS precipitation. Time series (left) and linear trends (right) of precipitation averaged within 3° of the vortex center for (a) monsoon lows and (b) monsoon depressions. Thick red and blue lines represent the multi-model means of the models having, respectively, extended-future projections to 2100 (the MRI-H and MRI-S models, MRI_mean) and near-future projections to 2050 (the full ensemble, MMM). Shading shows the spread across the models, time series are nine-year running means, the thin black line shows ERA5 values, and error bars represent a 90% confidence interval. (c) Projected changes in precipitation and specific humidity at 850 hPa, both averaged within 3° of the vortex center, as well as the projected change in the radial difference in MSLP between the surroundings and the storm's MSLP minimum. The horizontal dashed line marks the 7%/K rate of change. (d) Projected change in seasonal mean surface air temperature over the South Asian region ($10-25^{\circ}\text{N}$, $70-90^{\circ}\text{E}$). Bars with diagonal hatching represent changes between the historical (1980-2009) and extended-future periods (2070-2099), while bars without hatching represent changes between the historical and near future (2020-2049) periods.

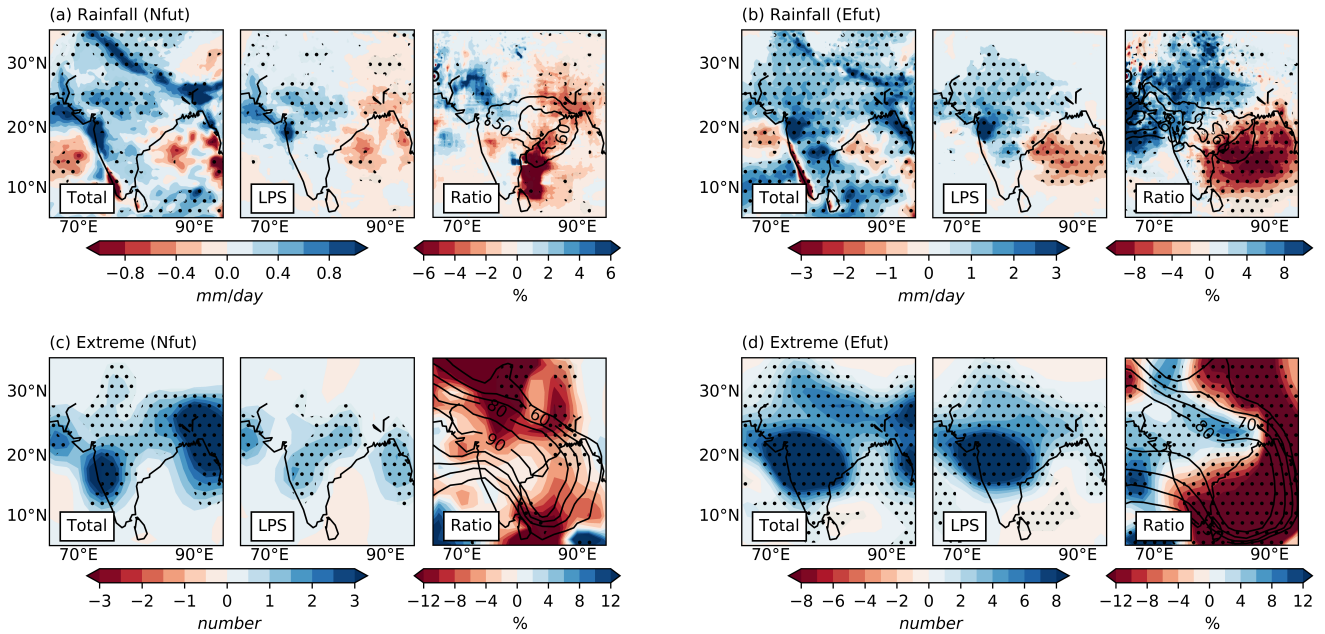


Figure 6. Changes in total, extreme, and LPS precipitation. (a) Projected changes between the historical (1980-2009) and near-future (2020-2049) periods of: total summer (June-September) precipitation (left), summer precipitation associated with LPS (middle), and the fractional contribution of LPS precipitation to total precipitation (right). Contours in the right panel show the percent contribution of LPS precipitation to total precipitation in the historical period. Panel (b) is the same as (a) but for changes between the historical and extended-future (2070-2099) periods. Panels (c) and (d) are the same as (a) and (b) but for the number of extreme precipitation events in a season, with an event defined as a day with precipitation greater than 150 mm. Stippling shows where at least 75% of the models have the same sign of change. The precipitation associated with LPS is the precipitation falling within 8° of the centers of all LPS, accumulated along the tracks of those LPS; extreme events associated with LPS are the total number of extreme events that occur within 8° of the storm center. Gaussian smoothing with radius of 4° is applied to plots of extreme event counts to reduce noise.